

Article

# Impact on Mechanical Properties and Microstructural Response of Nickel-Based Super-Alloy GH4169 Subjected to Warm Laser Shock Peening

Ying Lu<sup>1,2,\*</sup>, Yuling Yang<sup>3</sup>, Jibin Zhao<sup>1,2</sup>, Yuqi Yang<sup>1,2</sup>, Hongchao Qiao<sup>1,2</sup>, Xianliang Hu<sup>1,2</sup> and Jiajun Wu<sup>1,2</sup>, Boyu Sun<sup>1,2</sup>

<sup>1</sup> Shenyang Institute of Automation, Chinese Academy of Science, Shenyang 110016, Liaoning, China

<sup>2</sup> Institutes for Robotics and Intelligent Manufacturing, Chinese Academy of Sciences, Shenyang 110169, Liaoning, China;

<sup>3</sup> Northeastern University, Shenyang 110819, Liaoning, China

\* Correspondence: [luying@sia.cn](mailto:luying@sia.cn)

**Abstract:** Laser shock peening as an innovative surface treatment technology can effectively improve the fatigue life, surface hardness, corrosion resistance, and residual compressive stress. Compared with the laser shock peening, the warm laser shock peening (WLSP) is a new surface treatment technology to improve materials' surface performances, which takes advantage of thermal mechanical effects on stress strengthening and micro-structure strengthening, results in more stable distribution of the residual compressive stress under heating and cyclic loading process. In this paper, the microstructure of GH4169 nickel super-alloy processed by WLSP technology with different laser parameters were investigated. The proliferation and tangling of dislocations in GH4169 were observed and the dislocation density increased after WLSP treatment. The influences of different treatment by LSP and WLSP on the microhardness distribution of the surface and along cross-sectional depth were investigated. The microstructure evolution of the GH4169 alloy being shocked with WLSP were studied by TEM. The effect of temperature on the stability of high temperature microstructure and properties of GH4169 alloy WLP was investigated.

**Keywords:** warm laser shock peening (WLSP); GH4169 nickel-base super-alloy; microstructure; residual stress

---

## 1. Introduction

The Nickel-based super alloy has been widely used as turbine blades and disk links materials in aircraft, mainly due to their excellent thermal mechanical property stability, such as thermal fatigue, rupture ductility, oxidation resistance and creep strength. However, with the development of new aircraft engines, higher requirements for the mechanical properties were put forward to improve the service stability and service lifetime of the turbine blades or disks.

The investigations showed that temperature has an important influence on the flow stress of metal materials, mainly includes the following aspects [1-5]:

1. Dislocation motion: The increase of temperature enhances the thermal activation, and the concentration of vacancy defects reduces in the crystalline grain. The edge dislocation begin climbing, which prompts generation and annihilation of vacancy. The local equilibrium concentration of the dislocation is maintained, and the slippage movement of the screw dislocation also requires sufficient energy to activate.
2. Critical shear stress: The higher temperature leads to the critical shear stress of the material decrease, and the slip systems increase. With the increase of temperature,

atomic momentum becomes larger, and interatomic force is damaged, and then the shear stress reduced. There are more sliding positions, slip system is more active.

3. Organization of metal materials: As the temperature increases, solubility of solute atoms increases, which results in reducing the resistance of the alloy. The material thermoplastic and atomic thermal vibration are reinforced, and atoms in the lattice are unstable. In this state, the atoms are easy to move along the gradient of the stress field under the action of external forces, and the plasticity will be more strenuous.

It is clear that a more excellent mechanical property of the material can be achieved by increasing the temperature during treatments.

Warm laser shock peening (WLSP) combines the advantages of both laser shock peening (LSP) and dynamic strain aging (DSA), hence, WLSP technology can improve the fatigue properties of materials under alternating loads and high temperatures. WLSP is beneficial to stabilize the dislocation structure of the materials and suppressing the release of residual stress induced by LSP. Compared with the traditional LSP technology, WLSP is carried out under high temperature rather than room temperature, this in turn can achieve multi-faceted mechanical performance optimization [6-8]. By increasing the temperature, the dynamic strain aging occurs, a deeper residual stress layer on the surface of the material forms and the nano-precipitates generates, which results in a significant increase in the pinning effect on dislocation and the stability. Meanwhile, the density of the dislocation structure can be improved, and more stable residual compressive stress could be achieved by WLSP. Effectively suppress the effect of high temperature instability, Improve the high temperature stability of the material surface residual compressive stress layer, which is beneficial to improve the fatigue life. Hence, WLSP has been looked as a new and effective technology to improve the mechanical properties of the materials [9-11]. So far, most of the researches of WLSP strengthening technology are mainly focused on the low temperature alloy materials. It is well known that the high temperature alloys based on iron, nickel and cobalt are the key materials used for the hot end parts in the fields of aerospace, aviation, chemical industry and energy industry [12-14]. Hence, the investigations on improving the performances of such materials processed by WLSP are of major and immediate practical significance. The application of GH4169 superalloy was restricted under the temperature of 650 °C due to the coarsening and transformation of  $\gamma$  " phase processed under a higher temperature. Since the WLSP is carried out under 650 °C, the coarsening and transformation of  $\gamma$  " phase would be inhibited. Therefore, WLSP is a preferred technology to improve properties of GH4169. To our knowledge, few efforts were put on investigations on improving the surface structure stability and high temperature service performance of GH4169 superalloy by WLSP technique [15-17].

In present work, LP processing under 25 °C and WLP processing under 150°C, 200°C, and 250°C were carried out. The surface morphology, stress and microstructure of GH4169 alloy before and after LP and WLP processing were studied by theoretical and experimental methods. The effect of temperature on the stability of high temperature microstructure and properties of GH4169 alloy processed by WLP was investigated.

## 2. Experiment details

### 2.1. Materials and microstructure observation

Nickel-based GH4169 super-alloy was used as the experimental metallic materials. The chemical composition (wt. %) is 51.58 Ni, 18.36 Cr, 20.17 Fe, 2.96 Mo, 5.03 Nb, 0.99 Ti, 0.18 Si. In the alloy, Ni is the main element that forms the austenite matrix, and other elements, such as Fe and Co dissolved in the matrix, play a role of solid solution strengthening. The compounds formed with Nb and Ti can be precipitated as strengthening phase in the matrix. Meanwhile, the transition of the metastable  $\gamma$  " phase to equilibrium  $\delta$  phase could be inhibited by addition of Nb and Ti. In addition, the addition of Al, Ti, Cr and Mn has the function of improving the corrosion resistance and oxidation resistance of alloys. The specimen was cut into rectangular shape with size of 20 mm × 20 mm × 10 mm. The

surfaces were mechanically polished to eliminate residual tensile stress prior to the LSP treatment, and then peened by LSP roughly parallel to [001] orientation.

The samples for microstructure observation were mechanically polished and etched with a solution of 1.5 ml CuSO<sub>4</sub> + 40 ml HCl + 20 ml C<sub>2</sub>H<sub>5</sub>OH at room temperature. Image pro plus 6.0 OM was used to observe the microstructure.

### 2.2. Warm Laser shock peening process

The laser shock temperature was decided based on the formula of "qian – xiaoli model" proposed by Prof. Qian[18]. According to his theory, the temperature range of the dynamic strain aging of alloy is approximately  $0.2 \sim 0.5T_m$ , ( $T_m$  is the melting point temperature of an alloy). In this work, the melting temperature of GH4169 alloy is 1260 °C, hence, the dynamic strain aging temperature was calculated as 252 ~ 630 °C according to Qian's formula. Therefore, the temperature of warm laser shock peening selected in this study was 250 °C and 300 °C. As a contrast, the normal temperature of LSP was set as 25 °C.

A layer of aluminum foil sprayed with K9 glass with thickness of about 3mm was pasted on target surface as ablative layer. The glass layer prevented shock wave from spreading and prolonged the effect of shock wave. The samples were put on the pedestal, fixed by customized fixtures, and then heated to the setting temperature. The laser and robot were opened simultaneously as soon as the temperature reached the setting value. The processing was performed according to the default trajectory as illustrated in Fig. 1. The samples were removed after being cooled down to room temperature, and cleaned the surface with alcohol in the ultrasonic cleaner for 40 minutes.

The Nd:YAG laser system with wavelength of 1064 nm and average power of 130 W was used as the laser shock peening processing device. The laser parameters were set as pulse-width of 14 ns, pulse-energy of 5J, and repetition rate of 2 Hz. The spot diameter was focused to 2 mm. The heating system included heating pedestal, fixture, temperature sensor, Xmtd-3001 temperature controller and relay. The realization of the machining trajectory is achieved by the KUKA KR 270 R2900 ultra K model six axis robot, which ensured the precise motion of 0.1 mm in Cartesian coordinate system. The snake crawling trajectory used in WLSP experiment is shown in Fig.1.

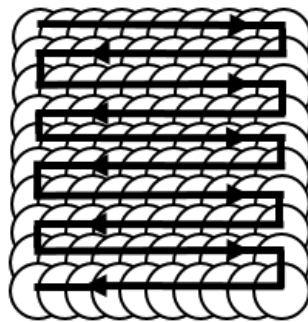


**Figure 1.** Snake crawling trajectory used in WLSP experiment.

### 2.3. Measurements of mechanical properties and microstructure

The surface residual stress was measured using D/Max-2500PC X-Ray diffraction equipment produced by Rigaku in Japan. The radiation source was CuK- $\alpha$ , the X-ray beam diameter was 1mm.

The microhardness of the shocked surface and cross-sectional depth was tested using a Micro Vickers Hardness Tester (DHV-1000) with a 0.98 N load and 10 s dwelling time. The microhardness along cross-sectional depth direction was measured at several positions with a distance of 10  $\mu$ m interval. In each location, three different points were selected to get the average value of the microhardness.

The evolution of microstructure of the samples was investigated by TEM (JEM-2100 JEOL) operated at 200 kV. The TEM samples were prepared by grinding the substrate to a thickness less

than 50  $\mu\text{m}$ , and polishing with a double-jet polisher at  $-35\text{ }^\circ\text{C}$  in a solution consisting of 10% perchlorate acid + 25% ethanol + 65% n-butanol.

The fatigue specimen were cut and cleaned ultrasonically for 20 min, and the fracture morphology was observed using SEM (JSM-6010LA, JEOL).

### 3. Results and discussion

#### 3.1. Surface morphology

The surface morphology was observed with light interference instrument and illustrated in Fig.2. As shown in Fig. 2a, uniform distribution of loose tissue defect and hard point bumps on the surface of GH4169 without peening was observed. The hard point bumps were formed by the strengthening carbide phase ( $\gamma, \gamma', \gamma'', \delta$ ), which were called the MC organization precipitated out during solidification. After being polished, these phase still maintain the shape of point bumps. The investigations showed that such characteristic of the tissue would contribute to high hardness and strong deformation resisting capability.

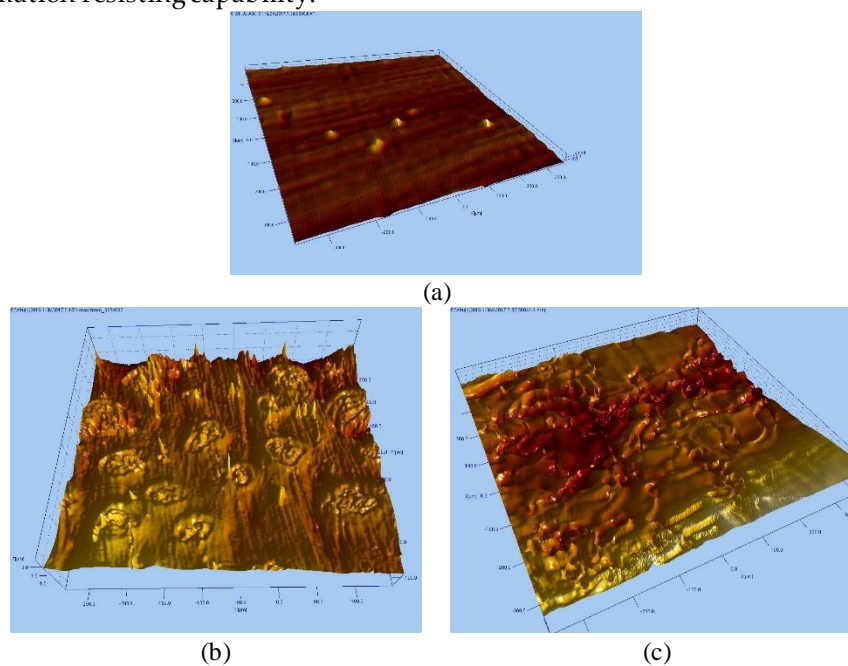


**Figure 2.** The surface morphology of different surface after treatment of (a) Original surface (b) LSP and (c) WLSP.

Fig. 2b and Fig.2c illustrated the surface morphology of the surfaces after being LSP and WLSP, respectively. Compared to the surface of the sample processed with LSP (Fig.2b), it is clear that no obvious relief structure was observed on the surface of the sample processed with WLSP as shown in Fig. 2c. Instead, a lot of surface ripples appeared, meanwhile, the ripples became more homogeneous with increasing of peening times and the laser energy, as illustrated in Fig.3. The surface roughness was quantitatively analyzed. According to the results of the ripples on the surface of the sample processed with WLSP as shown in Fig. 3b (peened 4 times), the roughness  $R_z$  was  $9.449\text{ }\mu\text{m}$ , and the depth reached  $1.5\text{ }\mu\text{m}$ , which could be easily distinguished. Compared with the surface reliefs peened at room temperature ( $R_z\text{ }1.8\text{ }\mu\text{m}$ ), the roughness for the samples processed with WLSP was much higher.

Surface reliefs by the laser shock is a common phenomenon at room temperature. There is no clear explanation for the phenomenon so far. Based on our researches, we concluded four possible explanations: during laser shock peening treatment, a plastic deformation delay occurred. The plastic deformation depends on the energy distribution of the laser. In this work, the temperature distribution of the laser beam can be characterized as Gaussian distribution. The uneven distribution of laser spot energy may result in uneven plastic deformation delay in different locations, this in turn

lead to the relief formation on the surface. Furthermore, a standing wave was formed between the constrained layer and sacrifice layer due to the wave superposition during LSP process. The uneven distribution of temperature field and energy of the standing wave lead to the formation of reliefs on the surfaces. Besides, the strengthening phase action may be another reason for relief's formation. In combination with the surface ripples formed by WLSP processing, the author prefers that the theory of strengthening phase play a major role in the evolution of surface topography of GH4169.

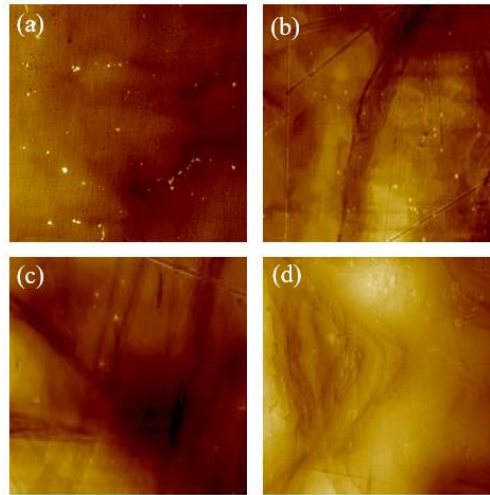


**Figure 3.** Local special surface morphology of specimen after WLSP. a) 300°C, 3J, 1 time, spot overlap rate 50%; b) 300°C, 3J, 4 times, spot overlap rate 50%; c) 300°C, 5J, 1 time, spot overlap rate 50%; d) 300°C, 5J, 4 times, spot overlap rate 50%.

### 3.2. The micro-hardness evaluation

As shown in Fig. 4, the micro-hardness for the base material is about 374HV0.1. The microhardness presents different values after WLSP at different temperature with same laser energy (5J) and same peened times.

The micro-hardness distribution along the cross-sectional depth direction was showed in Fig. 4. It was observed that the temperature had a great influence on the hardness value. The surface micro-hardness increased to 440 HV, 480 HV, and 492 HV, improved by 17.6%, 28.3%, and 31.6% after being processed with LSP temperature of 25°C (room temperature, RT), 250°C, and 300°C, respectively. It is obvious that the microhardness was much more significantly improved by WLSP than LSP at RT. The microhardness then gradually decreases along the cross-sectional depth to the value of the substrate region. The thickness of the hardened layer increased with increasing of the WLSP temperature. The hardened layer could reach 1.6 mm peened at 300°C, compared with the samples peened at room temperature was only about 1mm. The depth resulting from plastic deformation was proportional to the laser shock pressure. This nonlinear relationship between micro-hardness and plastic-deformation depth correction with the temperature and laser-induced shock pressure.

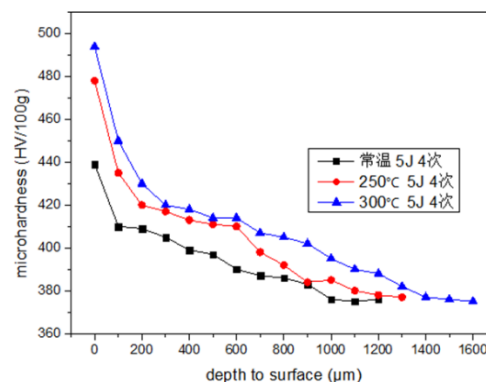


**Figure 4.** Microhardness distribution along cross-sectional depth direction.

The increase of the microhardness of the surface can be attributed to the formation of typical surface structure after LSP and WLSP treatment. As stated earlier, a plastic deformation occurred during LSP or WLSP, which result in the increasing of dislocation density and the refinement of the surface grains. Meanwhile, the plastic deformation, especially the high-speed plastic deformation resulted in the strain. The dislocation density, the refinement of the the grains and the stain due to the plastic deformation, in turn, enhanced the microhardness of the surface. However, the harden mechanism of WLSP differ from that of the LSP. Despite of the plastic deformation and grian refinement similar to LSP, the dynamic stain aging (DSA) is another important factor that improve the microhardness for WLSP treatment. It is well known that the highly dense  $\gamma''$  phase would be generated during WLSP due to high-speed deformation and dynamic precipitation. The volume density of  $\gamma''$  precipitates depends on the temperature and laser power. A higher temperature during WLSP can dramatically increase the volume density and provide higher thermal energy which will accelerate the precipitation process. A higher temperature provides a higher energy for the atoms to solute in the alloy.

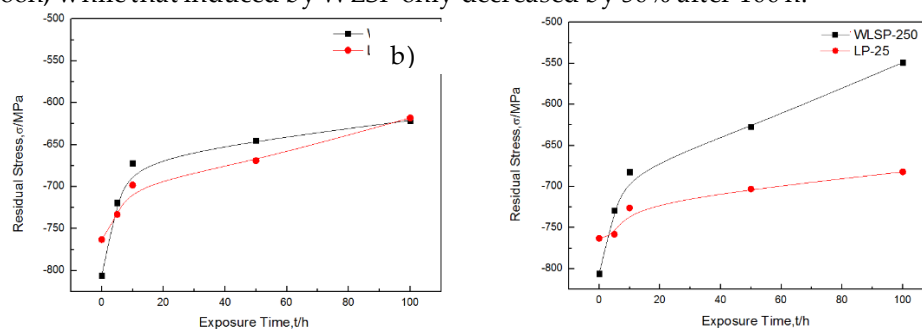
As rising of the temperature, the energy of the solute atoms in the alloy increase. The dislocation pinning will occur when the activation energy of the atoms is high enough and the moving speed of the atoms is less than that of the dislocation. This, in turn, leads to the accumulation and proliferation of the dislocation to get a higher dislocation density and grain refinement. The higher temperature results in the softening effect of the material, as well as the decreasing of the Elastic Modulus. So the microhardness of the surface increased significantly after peening. At the same time, the damping was reduced, resulting in the further propagation of the shock wavewithin the materials and the formation of a thicker surface strengthening layer.

### 3.3. The analysis of residual stress

With the purpose of evaluating the stability of the samples processed by LSP and WLSP, the residual stress at different temperature was measured by XRD method, the results are illustrated in Fig. 5 (The red line was the surface residual stress shocked by WLSP at 250 °C, and the black one was the surface residual stress shocked by LSP). It is observed that the surface residual stress due to WLSP is slightly lower than that of LSP at any aging temperature as shown in Fig. 5 a, b, and c (surface residual stress via exposure time at different temperature of (a) 600 °C, (b) 650 °C, and (c) 700 °C) . Similar trends were found for the samples processed at different aging temperature.

1. The surface residual stress shocked by WLSP was slightly lower than that of the surface shocked by LSP. However, the release of residual stress during the post-aging process induced by WLSP was less than LSP, indicating that the samples processed with WLSP is more stable than that processed with LSP.

2. The relaxation effects of the residual stress on the surface increased gradually with increasing of the aging temperature. No significant change in the surface residual stress was observed during the aging process at the temperature of 600 °C. The residual stress induced by LSP released completely, while that of WLSP only decreased by 8% when the aging temperature increased to 650°C. Moreover, when the aging temperature increased to 700°C, the residual stress induced by LSP released soon, while that induced by WLSP only decreased by 50% after 100 h.



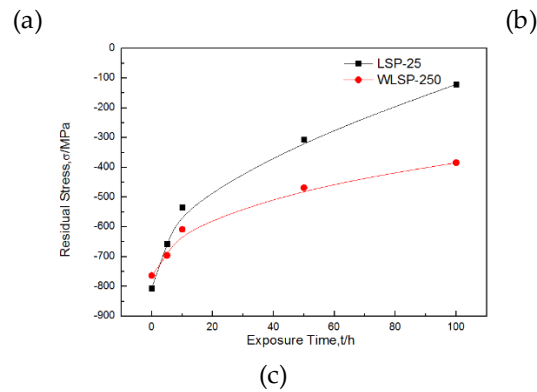


**Figure 5.** Surface residual stress via exposure time at different temperature of (a) 600 °C, (b) 650 °C, and (c) 700 °C.

It was found that both the residual stress and the dislocation density increased due to the increasing of temperature and the laser intensity. On the one hand, with the increasing of the aging temperature, the motion resistance of dislocation decreased, the dislocation entanglement gradually expanded, and dislocation rearrangement and annihilation appeared, which resulted in a decrease of dislocation density and lattice distortion. With the increasing of the temperature, the residual stress relaxed rapidly. On the other hand, the increasing of the aging temperature resulted in increasing of the grain size of the  $\gamma''$  phase and the transformation of  $\gamma''$  phase to  $\delta$  phase. The results are in accordance with the surface hardness tests result. The results further confirm that the enhanced pinning effect caused by a higher volume density of  $\gamma''$  precipitates is responsible for the temperature and laser intensity effects on the hardening ratio. As a result, the strength and resistance of the material decreased quickly with the wide relaxation of the residual stress during aging procedure under a high temperature. The magnitude and stability of laser-induced residual stress played critical roles on the determination of the fatigue performance of metallic materials. In summary, the higher the aging temperature, the better thermal stability of the stress/tissue produced by WLSP.

#### 3.4. The microstructure analysis

It is well known that the properties of a certain material depends on its microstructure. The nickel-based GH4169 super alloy is mainly composed of the  $\gamma$  phase (fcc) as the matrix, auxiliary reinforcement phase  $\gamma'$ -Ni<sub>3</sub>Al (fcc, inter-metallic compounds with L1 structure), reinforcement phase  $\gamma''$ -Ni<sub>3</sub>Nb (bct, inter-metallic compounds with DO<sub>22</sub> structure), and  $\delta$  phase (stable phase with DO<sub>3</sub> structure). There will be a transformation from  $\gamma''$  phase to stable  $\delta$  phase during a long-time aging processing or serving. Accordingly, the strength will reduce sharply. The TEM observation results (Fig 6a and 6b) illustrated that the internal part of GH4169 after stress relief annealing presented less dislocation density, and a little amount of lattice distortion distributed around the partially reinforced phase. A little amount of disk-shaped  $\gamma''$  phase and granular  $\gamma''$  phases distributed in the crystal were observed. Besides, a large amount of spherical or plate-like  $\delta$  phase precipitates were also observed on the grain boundaries. We deduced that such highly "tangled" structures would be beneficial for the stability of mechanical properties at high temperature (about 650 °C). When the dislocation density reaches a certain threshold, dynamic recrystallization occurs at grain boundaries, shear bands and impurities, which promotes the dynamic precipitation or refinement of strengthening phases.

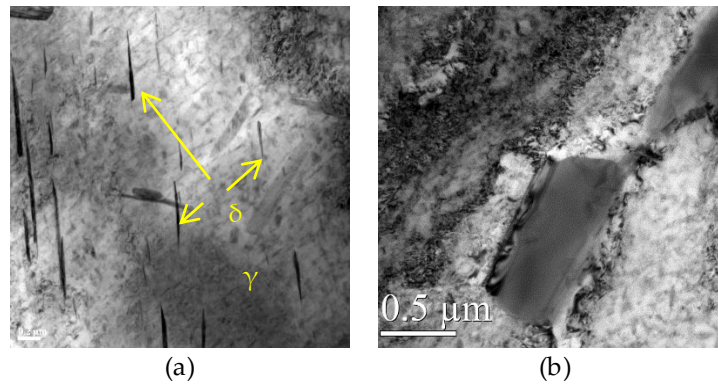


**Figure 6.** The main phase composition of GH4169.

The appearance of DSA and DP on the surface of the material during WLSP would affect on the microstructure and in turn improve its properties. By comparing the differences in Fig. 7, Fig. 8, and Fig.9, we can concluded as following:

(1) Different from the structures in Fig.6 corresponding to the sample before peening, there were a large number of complex dislocations structures in matrix  $\gamma$  phase after laser shock peening (Fig. 7a). After LSP, the dislocation organization increased obviously, the dislocation density increased greatly, and many sub-structures were formed. The red line illustrated in Fig. 7a showed the direction of grain deformation under laser shock, and the yellow lines represent the direction of dislocations in the  $\gamma$  phase matrix. The angle between red line and yellow line is approximately  $90^\circ$ . The dislocations in  $\delta$  phase were produced in large quantities at the edge of grain boundaries and moved towards the interior of grains (Fig. 8a). It is observed that dislocation twins appeared along the long axis direction of the  $\delta$  phase. The twin formed along the same direction with the dislocation movement. A large number of dislocations accumulated at the grain boundaries, and the aggregation of dislocations at the grain boundaries might further caused the grain boundary deflection (Fig. 9a). A large number of dislocations lines appeared in the phase and moved along the grain boundaries. The accumulation of the large number of dislocations at the grain boundaries may further caused the grain boundary deflection.

(2) The peening under high temperature in the process of WLSP resulted in the continuous accumulation of dislocations in the  $\gamma$  phase matrix, and formation of a large number of entangled dislocations (Fig.7b). The amounts of the dislocations and its density in the samples processed by WLSP increased by a large margin compared to the sample processed by LSP. The effect of dislocation on grain or grain boundaries was more obvious, and lots of dislocations gathered near the grain boundaries. Especially when the temperature reached  $150^\circ\text{C}$  (Fig.9b), the dislocation accumulation caused a significant deflection of the grain boundaries. When the samples were shocked at the temperature of  $200^\circ\text{C}$  (Fig.9c), some of the crystal boundaries darkled away so that it was difficult to identify them due to the action of dislocations. The concentration of dislocation structures could provide nucleation sites for phase precipitation, which was beneficial to dynamic precipitation (Fig.10b).

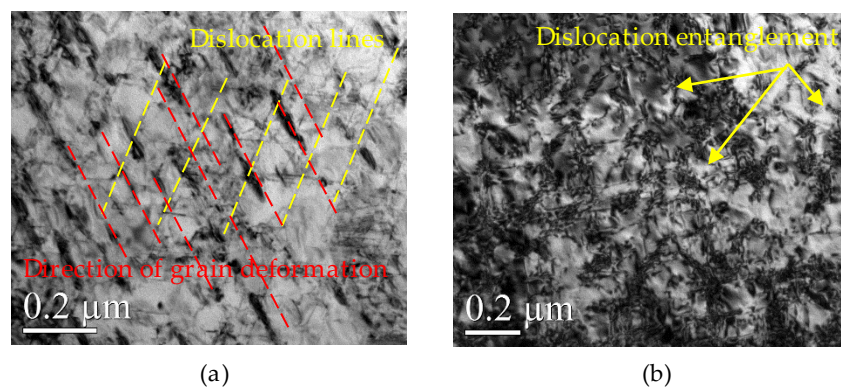


**Figure 7.** The change of  $\gamma$  phase shocked by LSP at different temperature. (a) 25°C, (b) 200°C.

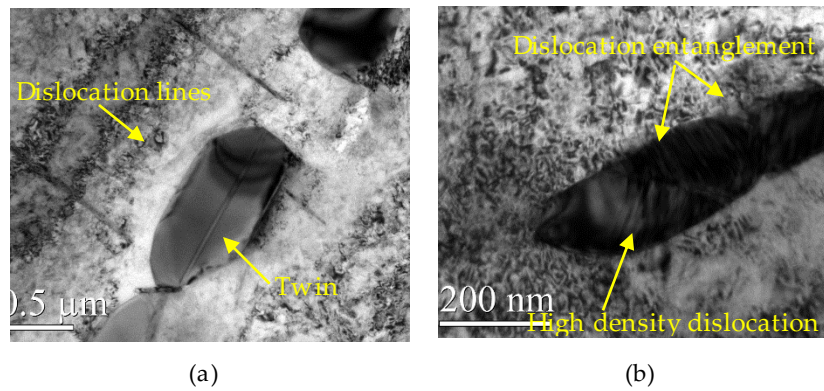


**Figure 8.** The change of  $\delta$  phase shocked by LSP at different temperature: (a) 25°C, (b) 200°C.

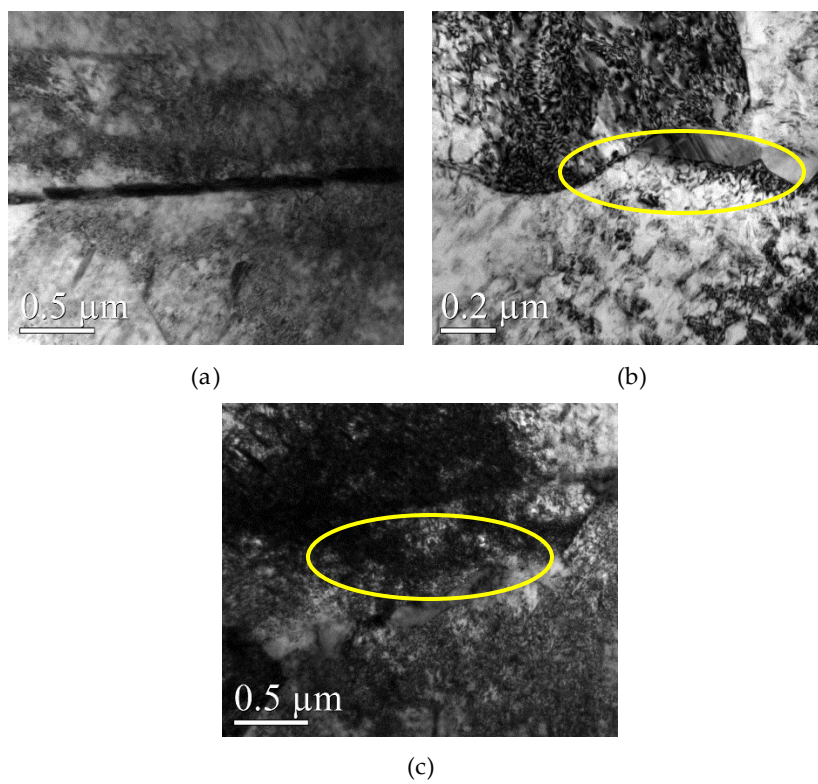


**Figure 9.** The change of grain boundary shocked by LSP at different temperature: (a) 25°C, (b) 150°C, (c) 200°C.

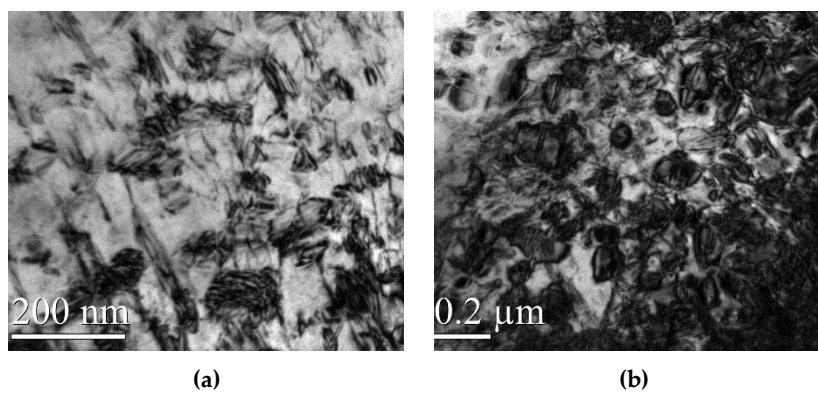


**Figure 10.** The change of  $\gamma'$  phase shocked by LSP at different temperature: (a) 25°C, (b) 200°C.

During laser shock peening, the dislocations moved towards a single direction and eventually gathered at the grain boundaries. Then they were blocked by the boundaries and resulted in the formation of twins, sub-grain boundaries and new grain boundaries. Ultimately, a large number of crystal defects were formed. These defects moved and aggregated, a part of them formed a sub-grain boundary at a small angle. When they moved to the phase interface, they were pinned by the interface surface, the migrations of the sub-grain boundaries were obstructed, which could eventually lead these sub-grain boundaries to gather at the phase boundary. The grain boundaries would be deflected under the interaction of the phase boundaries and the surface tension of the sub-grain boundaries to balance the surface tension. (The aggregating dislocation morphology was as shown in Fig. 9b).

It is well known that the strengthening  $\gamma''$  phase is a metastable phase. It will coarsen and transfer to a  $\delta$  stable phase under a high temperature condition. The transformation then leads to the rapid change of strength and creep property. The  $\gamma''$  phase precipitated in the  $\delta$  phase retarded the dislocation motion and the nucleation and growth of the recrystallized grains. Meanwhile, the accumulation of the dislocation limited the growth of the  $\delta$  phase. As stated earlier, the surface processed by WLSP presented more excellent high temperature stability in residual stress than that processed by LP. The reason is the DSA phenomenon caused by increasing of temperature. Although the resistance of dislocation motion decreased at high temperature, the solute atoms diffused quickly enough to catch up with the motion of the dislocations to form a mass of solute atoms with large size enough to pin the dislocations. The reduction of the movable dislocations promoted the proliferation of a large number of dislocations, and finally increased the density of the dislocations. Meanwhile, the dislocation annihilation negative effect caused by dynamic recovery was the smallest, and the dislocation density also kept a larger value at high temperature, which improved the high temperature stability of the material. The pinning effect of secondary phases in GH4169 alloy was analyzed and could be concluded that the precipitated  $\gamma''$  phase within the grains retained the dislocation motion, the precipitated  $\gamma''$  phase in  $\delta$  grains hindered the nucleation and growth of recrystallized grains, the dislocations limited the  $\delta$  grain growth.

Compared with the bright and dark field of microstructure features shocked by WLSP and LSP (Fig. 11), a certain number of dislocations were accumulated in the  $\gamma''$  phase, and a large number of sub-phases appeared in the  $\gamma''$  phase, which finally led to the disc-shaped  $\gamma''$  phase were cut off. The  $\gamma''$  phase (the size were about 100 nm) was cut into a smaller size of  $\gamma'$  phases (the size were about 30 nm). This phenomenon can be explained as following.

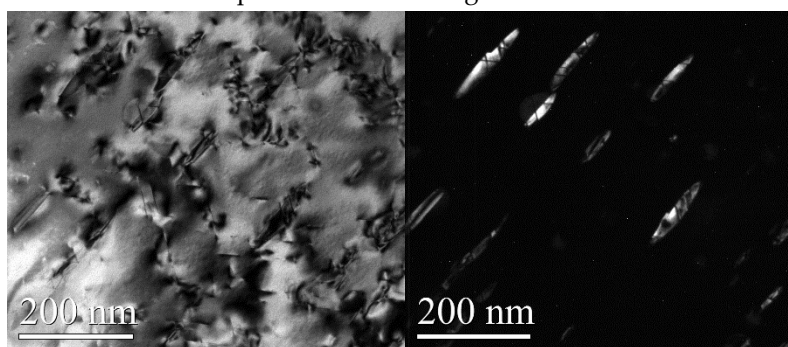


**Fig.11** The comparison of the light field phase and the dark field phase of  $\delta$  phase shocked by LSP at 200°C

First, due to the pinning effect of precipitates on dislocations and the effect of dislocation proliferation, high strain rate deformation produced higher dislocation density at that temperature. At the same time, the surface plastic deformation of the material was strengthened, which promoted the appearance of super vacancy. The diffusion of the vacancy atom in the thermal insulation process reduced the system energy, which resulted in the non-equilibrium segregation of Nb, the increasing of the nucleation position of the  $\gamma''$  phase, and the nucleation rate of the  $\gamma''$  phase in strengthening layer. The plastic deformation caused by WLSP promoted the appearance of super vacancy. The vacancy formed in WLSP process combined with the Nb atoms to form a vacancy-Nb pair. The

vacancy-Nb pair diffused towards the defect and reduced the system energy, resulting in the Nb non-equilibrium. Because the driving force of this concentration gradient would lead to the movement of the  $\gamma''/\delta$  interface, the heat treatment at a lower temperature would promote the expansion and spheroidization of the decomposed  $\alpha$  phase.

Because the plastic deformation at warm temperature caused plastic deformation on the surface of the material, which could lead to the appearance of supervoids. In the process of WLSP, the vacancy combined with the -Nb atom to form the vacancy-Nb pair. The concentration gradient forces caused the  $\gamma''/\delta$  interface to move, and the decomposed  $\delta$  phases expanded and spheroidized at lower temperatures (the relationship between the grain boundary phase and its adjacent phase satisfied the orientation relation of Burgers.)

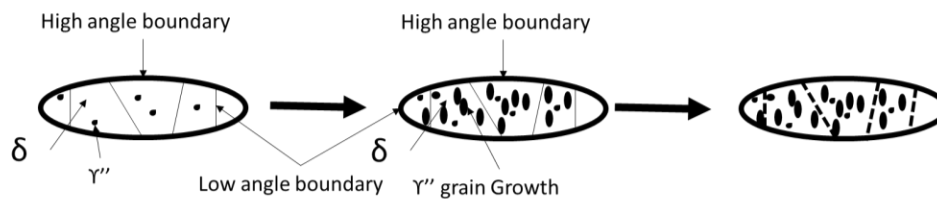


**Figure 12.** The  $\gamma''$  grain deposition and the  $\delta$  phase refinement in GH4169 alloy.

On the other hand, the decomposition of  $\gamma''$  phase effect introduced by WLSP promoted the precipitation of high-density of nanoscale particles. The tangled dislocation band and the strength phase effectively inhibited the movement of dislocations by its pinning effect, which contributed to enhance the material stability at high temperature. After the decomposition, the dislocations climbed and slipped inside the matrix phase. Uniform dislocations were rearranged as smaller angle grain boundaries or sub-grain boundaries perpendicular to the sliding surface, and the inhomogeneous dislocations were counteracted by each other, eventually increased the number of the sub-grain boundary area, which could lead to the grain size decreased and the surface hardness and yield strength increased. (The influence of strength grain size on the yield flow stress and hardness was usually written in the form of the Hall–Petch). The precipitated relative dislocation played a pinning role, and the accumulation of dislocation provided more nucleation sites for the precipitated phase. WLSP decreased the phase content and the pinning force to grain boundary migration. The dislocations in the elongated grains are clustered near the phases. The small-angle grain boundaries in the elongated grains form new large-angle grain boundaries through migration and rotation, and the original elongated grains are divided into several smaller equiaxed grains. Thus, the finely dispersed and dispersed  $\gamma''$  phase was interspersed with a large number of dislocations in the  $\delta$  phase, forming a structure similar to reinforced concrete. This structure could be very stable at high temperatures, and the high-temperature stress release process, the dislocations had excellent pinning effect and effectively improved softening resistance and creep resistance at high temperature.

#### 4. Conclusions

In this paper, the microstructure of GH4169 nickel super-alloy processed by WLSP technology with different laser parameters were investigated. The proliferation and tangling of dislocations in GH4169 were observed and the dislocation density increased after WLSP treatment. The influences of different treatment by LSP and WLSP on the microhardness distribution of the surface and along cross-sectional depth were investigated. The microstructure evolution of the GH4169 alloy being shocked with WLSP were studied by TEM. The effect of temperature on the stability of high temperature microstructure and properties of GH4169 alloy WLP was investigated, and the analysis was as follows:

(1) Compared with LSP, WLSP could obtain more complex dislocation structure, the dislocation promoted the precipitation of enhanced phase, this in turn enhanced the pinning effect of dislocation. The effect of dislocation on grains or grain boundaries was more obvious, and lots of dislocations gathered near the grain boundary, especially when the temperature reached 150 °C, the

dislocation accumulation caused a significant deflection of the grain boundary. When the samples shocked at 200 °C, with the action of dislocations, some of the crystal boundaries have been blurred and it was difficult to identify them. A large concentration of dislocation structures could provide nucleation sites for phase precipitation, which was beneficial to dynamic precipitation (DP).

(2) One hand, The surface plastic deformation of the material was strengthened, which promoted the appearance of super vacancy. The diffusion of the vacancy atom in the thermal insulation process reduced the system energy, which caused the non-equilibrium segregation of -Nb, and increased the nucleation position of the  $\gamma''$  phase. Thereby, the nucleation rate of the  $\gamma''$  phase in strengthening layer was increased. On the other hand, uniform dislocations were rearranged as smaller angle grain boundaries or subgrain boundaries perpendicular to the sliding surface, and the inhomogeneous dislocations were counteracted by each other, eventually increased the number of the subgrain boundary area, which could lead to the grain size decreased and the surface hardness and yield strength increased.

(3) The precipitated relative dislocation played a pinning role, and the accumulation of dislocation provided more nucleation sites for the precipitated phase. Thus, the finely dispersed and dispersed  $\gamma''$  phase was interspersed with a large number of dislocations in the  $\delta$  phase, forming a structure similar to reinforced concrete. This structure could be very stable at high temperatures, and the high-temperature stress release process, the dislocations had excellent pinning effect and effectively improved softening resistance and creep resistance at high temperature.

**Funding:** This study was NSFC-Liaoning Province united foundation (No. U1608259).

**Acknowledgments:** The authors thank the anonymous reviewers for their critical and constructive review of the manuscript.

**Conflicts of Interest:** The authors declare that there are no competing interests regarding the publication of this paper.

## References

1. X. Nie, W. He, S. Zang, X. Wang, J. Zhao, "Effect study and application to improve high cycle fatigue resistance of TC11 titanium alloy by laser shock peening with multiple impacts," *Surface and Coatings Technology*, **253**(0),68-75(2014). Investigation on Residual Stress Loss during Laser Peen Texturing of 316L Stainless Steel
2. B. Pant , R. Sundar, H. Kumar, R. Kaul, A. Pavan, "Prakash. Studies towards development of laser peening technology for martensitic stainless steel and titanium alloys for steam turbine applications," *Materials Science and Engineering: A*, **587**,352-358(2013).
3. I. Altenberger, R. K. Nalla, Y. Sano, L. Wagner, R. O. Ritchie, "On the effect of deep-rolling and laser-peening on the stress-controlled low- and high-cycle fatigue behavior of Ti-6Al-4V at elevated temperatures up to 550°C," *International Journal of Fatigue*, **44**,292-302 (2012).
4. Y. Ji, S.Wu, "Study on microstructure and mechanical behavior of dissimilar Ti17 friction welds," *Materials Science and Engineering: A*, **596**, 32-40 (2014) .
5. J. S. Zhou, L. Huang, X. Zuo, J. Meng, Q. Sheng, Y. Tian, W. Z. Han, "Effects of laser peening on residual stresses and fatigue crack growth properties of Ti-6Al-4V titanium alloy," *Optics and Lasers in Engineering*, **52**,189-194 (2014) .
6. S. Spanrad, J. Tong, "Characterisation of foreign object damage (FOD) and early fatigue crack growth in laser shock peened Ti-6Al-4V aerofoil specimens," *Materials Science and Engineering: A*, **528**(4),2128-2136(2011).

7. Y. J. Sano, M. Obata, T. Kubo, N. Mukai, M. Yoda, "Retardation of crack initiation and growth in austenitic stainless steels by laser peening without protective coating," *Materials Science and Engineering: A*, **417**(1-2), 334-340(2006).
8. S. M. Zabeen, P. W. Preuss, "Evolution of a laser shockpeened residual stress field locally with foreign object damage and subsequent fatigue crack growth," *Acta materialia*, **83**,216-226(2015).
9. B. J. Wu, L. Zhang, Y. S. Zhang, Y.S. Pyoun, R. Murakami, "Effect of ultrasonic nanocrystal surface modification on surface and fatigue properties of quenching and tempering S45C steel," *Applied Surface Science*, **321**,318-330(2014).
10. J. J. Wu, X. J. Liu, J. B. Zhao, "The online monitoring method research of laser shock processing based on plasma acoustic wave signal energy," *Optik*, **183**,1151-1159(2019).
11. K. Y. Luo, T. Lin, F. Z. Dai, "Effects of overlapping rate on the uniformities of surface profile of LY2 Al alloy during massive laser shock peening impacts," *Surface & Coatings Technology*, **266**,49-56,(2015)
12. F. Z. Dai, Z. D. Zhang, X. D. Ren, "Effects of laser shock peening with contacting foil on micro laser texturing surface of Ti6Al4V," *Optics And Lasers In Engineering*, **101**,99-105(2018).
13. K. M. Li, Y. F. Wang, Y Cai, "Investigation on Residual Stress Loss during Laser Peen Texturing of 316L Stainless Steel," **9**(17), (2019).
14. Y. L. Liao, C. Ye, G. J. Cheng, "Warm laser shock peening and related laser processing technique," *Optics & Laser Technology*, **78**,15-24(2016).
15. J. Z. Lu, K. Y. Luo, Y.K. Zhang, G. F. Sun, Y. Y. Gu, J. Z. Zhou, X. D. Ren, "Grain refinement mechanism of multiple laser shock processing impacts on ANSI 304 stainless steel," *Acta Materialia*, **58**(16): 5354-5362, (2010).
16. X. D. Ren, Z. P. Tong, W. F. Zhou, "High temperature wear performance of Ti-6.5Al-3.5Mo-1.5Zr-0.3Si alloy subjected to laser shock peening," *Materials Science And Technology*, **34**(18),2294-2304(2020).
17. G. X. Lu, J. D. Liu, Y. Z. Zhou, T. Jin, X. F. Sun, Z. Q. Hu, "Differences in the micromechanical properties of dendrites and interdendritic regions in superalloys," *Philosophical Magazine Letters*, **55**,1-8(2016).
18. H. Zhang, Z. H. Ren, J. Liu, "Microstructure evolution and electroplasticity in Ti64 subjected to electropulsing-assisted laser shock peening," *Journal of Alloys and Compounds*, **802**(25), 573-582(2019).
19. X. N. Hou, S. Mankoci, N. Walters, "Hierarchical structures on nickel-titanium fabricated by ultrasonic nanocrystal surface modification," *Materials Science & Engineering*, **98**,1307-1307 (2019).
20. J. Li, J. Zhou, and A. X. Feng, "Twin formation and its strengthening mechanism of pure titanium processed by cryogenic laser peening," *Optics And Laser Technology*, **120**, 105763(2019).



© 2020 by the authors. Submitted for possible open access publication under the terms and conditions of the Creative Commons Attribution (CC BY) license (<http://creativecommons.org/licenses/by/4.0/>).